EASR

Engineering and Applied Science Research

https://www.tci-thaijo.org/index.php/easr/index

Published by the Faculty of Engineering, Khon Kaen University, Thailand

Computational analysis of water-based copper oxide nanofluid properties and performance in a double-pipe small-scale heat exchanger

Sulaiman Musediq A.*[1)], Aminu Yahaya[1)], Olatunde Olanrewaju B.[1)], Adetifa Babatunde O.[2)] and Giwa Solomon O.[1)]

[1)]Department of Mechanical Engineering, Faculty of Engineering, College of Engineering and Environmental Studies, Olabisi Onabanjo University, 112104, Ibogun, Ogun State, Nigeria
[2)]Department of Agricultural Engineering, Faculty of Engineering, College of Engineering and Environmental Studies, Olabisi Onabanjo University, 112104, Ibogun, Ogun State, Nigeria

Received 19 March 2020
Revised 23 July 2020
Accepted 29 July 2020

Abstract

This paper models the thermal transport properties and performance of a water-based CuO nanofluid (with varying volume fractions of CuO) in a laboratory-sized double pipe heat exchanger (DPHE). Copper oxide (CuO) nanoparticles were used and their quantity was varied from a volume fraction of 0% to 0.1% with an incremental step size of 0.025%. The mass flow rates of the hot and cold fluids were maintained at 0.87 kg/s and 0.9 kg/s, respectively. Simulation results revealed that temperatures of 410 and 306.75 K, respectively, were attained at the hot and cold fluid outlets. Analysis of the DPHE showed that for cold fluids, thermophysical properties such as viscosity, thermal conductivity, specific heat capacity (SHC) and density were enhanced by the addition of nanoparticles. The temperature distribution, effectiveness and the heat transfer in the DPHE were observed to linearly increase with increment increases of the nanoparticle volume fraction.

Keywords: Nanoparticles, Heat transfer, Heat exchanger, Thermal properties, ANSYS

1. Introduction

Efficient heat energy use and transfer is a challenging problem affecting many industries today. This can be addressed through effective improvement of heat transfer processes by employing heat exchangers [1, 2] using various auxiliary technologies. One of these is a passive augmentation technique that involves addition of nanoparticles into the base fluid [3-6].

Nanofluids have properties that are useful in practical applications. As a result of their desirable characteristics, they improve the performance of heat transfer fluids [7]. They have been applied in numerous fields and perform well in heat exchangers [8]. Nanoparticles with diameters less than 50 nm have been shown to improve the properties of a base fluid by increasing their thermal conductivity [7]. They have also been reported to increase the convective and conduction heat transfer coefficients, enhancing heat exchanger performance [9]. Unlike heat transfer enhancement using large suspended particles, nanoparticles in the fluids usually exhibit improved properties that promote heat transfer at very low concentrations as a result of their small sizes [10]. The behaviour of various nanofluids has been investigated in numerous studies employing several numerical methods to identify the effects of these nanofluids on heat transfer mechanisms [11-15].

Huminic and Huminic [16] reviewed the application of nanofluids in heat exchangers and reiterated that large energy costs influence the decisions of various industries to adopt energy-saving technologies as much as possible for various unit operations and production processes. In previous studies, research efforts have been geared towards enhancement of thermal transport properties and mechanisms of heat exchangers. They aimed at reducing the time for heat transfer thereby improving the thermal performance of the heat exchangers [3, 6]. Nanofluids that are prepared from sonication of metals or metal oxide particles in a base fluid, like water [17-20], have been investigated in several studies to identify their effects in different types of heat exchangers [21-26].

The heat transfer coefficient of nanofluids flowing through a vertical pipe was studied by Tiwari et al. [21]. They observed increased heat transfer at larger Reynold's numbers and volume fractions of nanoparticles. Particle concentration has more effect on the Reynold's number, especially when the flow regime is turbulent. Studies have shown that the volume fraction of nanoparticles and Reynold's number increase the Nusselt number while the friction factor can either decrease [23] or increase [24], depending on the type of nanoparticles used.

Demir et al. [23] reported enhanced thermal transport characteristics for TiO_2/water nanofluids in a double tube counter-flow heat exchanger using single-phase forced convection. Ghalib et al. [25] investigated the thermal effect of a ZrO_2/water nanofluid in a double pipe heat exchanger. Improved thermal transport properties of the fluid were reported resulting from the presence of the nanoparticles. Huminic and Huminic [26] reported the use of CuO and TiO_2 nanoparticles (24 nm) added to water at volume concentrations of 0.5 – 3.0 vol.% in a double tube helical heat exchanger. There was a 14-19% increase in the rate of heat transfer, depending on whether the flow was annular or tube flow.

Shirvan et al. [27] did a numerical analysis on the effectiveness of a double pipe heat exchanger (DPHE) through

*Corresponding author.
Email address: sulaimanadedoyin@oouagoiwoye.edu.ng
doi: 10.14456/easr.2021.18

Table 1 The thermal properties of copper oxide

S/N	Property	Value
i.	Thermal conductivity (W/m.K)	33
ii.	Specific heat (Kg/.K)	0.531
iii.	Density (Kg/m^3)	6400

Table 2 Properties of the fluids considered

S/N	Property	Hot fluid (water)	Cold fluid (Ø=0)
i.	μ (10^{-3} kg/m.s)	0.21	0.84
ii.	k (W/m.K)	0.687	0.609
iii.	C (kJ/kg.K)	4.268	5.770
iv.	ρ (kg/m^3)	932.5	1000

Key: μ-dynamic viscosity, k-thermal conductivity, C- specific heat, and ρ-density

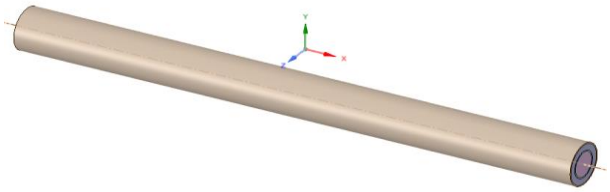

Figure 1 A simple DPHE

which an Al_2O_3/water nanofluid flowed using a response surface methodology. This study revealed that the effectiveness of the DPHE was enhanced with an increase in the volume fraction of Al_2O_3 nanoparticles in the nanofluid and reduced with an increase in the pipe diameters used to flow the nanofluid. These findings were in agreement with the report of a numerical simulation of Mozafarie et al. [28] using a DPHE enhanced with circular fins in which an Al_2O_3/water nanofluid was flowed. Similarly, Bahmani et al. [29] observed that for turbulent heat transfer while flowing an Al_2O_3 nanofluid in a DPHE, the fluid outlet temperature, DPHE wall temperature, Nusselt number and convective heat transfer coefficient increased with the volume fraction of Al_2O_3 in the nanofluid. Other studies reported similar results for DPHEs enhanced using various volume fractions of nanofluids such as Fe_3O_4 [30], ZnO [31, 32], MgO/water-ethylene glycol [33], multi-walled carbon nanotubes (MWCNT) [34-36], graphene nanosheets [34], and MWCNT-Fe_3O_4/water [37], among others.

According to Omidi et al. [38], any imperative to transform and improve the effectiveness of DPHEs should be geared towards decreasing the size and cost of the heat exchanger. This showed that there is a need for further studies at various nanofluid volume fractions, as well as in different types and scales of heat exchangers. Some of the studies done in laboratory scale DPHEs used no nanofluid enhancement. Hence, the objective of improving the effectiveness of the heat exchanger was not realized [39]. This work, therefore, models the thermal performance and effectiveness of a laboratory-scale double pipe heat exchanger using a water-based copper oxide nanofluid at varying volume fractions. A mesh study was performed and analysis of the various volume fractions of the nanofluid on heat transfer was studied using ANSYS.

2. Materials and methods

The materials used in this study were comprised of the solid and fluid components that made up the system. The heat exchanger was made of aluminium, while water was flowed in both the hot and cold pipes. Copper oxide (CuO) nanoparticles were added to the cold fluid to enhance its thermophysical properties. Mathematical models were used in estimating the thermal properties of the nanofluid as a function of the base fluid and amount of nanoparticles added. The quantity of nanoparticles dispersed into the base fluid was also varied to control its volume fraction. Table 1 presents the thermal conductivity, specific heat, and density of CuO nanoparticles, while those of the cold (with varying nanoparticle volume fractions) and hot fluids are presented in Table 2. The range of volume fractions used in this study was selected to enable comparison with the values reported in several other studies [40-42].

2.1 Nanofluid properties

A. Dynamic viscosity: An empirical model (Equation 1) presented by Brinkman [43] was used in determining the dynamic viscosity of the nanofluids.

$$\mu_{nf} = \frac{\mu_{bf}}{(1-\emptyset)^{2.5}} \tag{1}$$

where μ_{nf}, μ_{bf} and $\emptyset$ are the viscosity of the nanofluid, base fluid and the volume fraction of CuO respectively.

B. Thermal conductivity: This was estimated with the model of Mintsa et al. [44]. Equation 2 was used to determine the thermal conductivity of the nanofluid using the thermal conductivity of the base fluid (water) and the thermal conductivity and volume fraction of the nanoparticle material (CuO).

$$k_{nf} = k_{bf} + 3\emptyset\left(\frac{k_p - k_{bf}}{2k_{bf} + k_p - \emptyset(k_p - k_{bf})}\right)k_{bf} \tag{2}$$

where k_{nf}, k_{bf}, and k_p are the thermal conductivities of the nanofluid, base fluid and nanoparticle material, respectively.

C. Specific Heat Capacity (SHC): This was estimated with a nanofluid model (Equation 3) to determine specific heat using the SHC of the base fluid (water) and the SHC of the volume fraction of the nanoparticle material (CuO) as reported by Zhou and Ni [45]. For rapid heat build-up, the SHC of the nanofluid should be lower than that of the base fluid.

$$C_{nf} = \emptyset C_p + (1-\emptyset)C_{bf} \tag{3}$$

where C_{nf}, C_{bf} and C_p are the SHC values of the nanofluid, base fluid and nanoparticle material, respectively.

D. Density: Incompressible fluid flow occurs at a constant density. The density of nanofluid depends on both that of the base fluid and the nanoparticles as well as the nanoparticle volume fraction. This was computed using the empirical expression of Pak and Cho [46] (Equation 4).

$$\rho_{nf} = \emptyset\rho_p + (1-\emptyset)\rho_{bf} \tag{4}$$

where ρ_{nf}, ρ_{bf} and ρ_p are the densities of the nanofluid, base fluid and nanoparticle material, respectively.

2.2 System description

The geometry used in this study was a simple double pipe heat exchanger (DPHE) (Figure 1) which was comprised of two concentric pipes with circular cross-sections. A hot fluid was conveyed through the inner pipe, while the coolant fluid flowed in the space/cavity created between the inner and outer pipes (Figure 2).

The dimensions the DPHE used in the current study are presented in Table 3. No baffles were used in this apparatus.

2.3 Governing equations

The models used in this study employed fundamental fluid dynamics and heat transfer equations for incompressible fluid

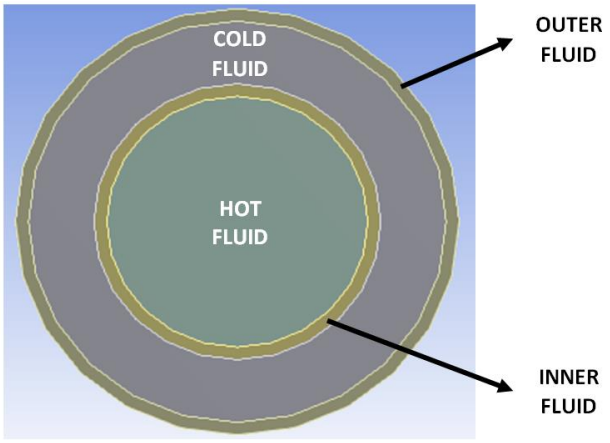

Figure 2 The cross-section of the DPHE

Table 3 Dimensions of the DPHE in the current study

Parameter	Dimension (m)
Length	1.000
External pipe outer diameter	0.085
External pipe inner diameter	0.080
Inner pipe outer diameter	0.055
Inner pipe inner diameter	0.050

flow. They included the three-dimensional continuity equation (Equation 5) to account for a constant mass flow rate, the three-dimensional momentum equations for fluid flow (Equation 6, 7, and 8) and the three-dimensional energy equation that accounted for the heat flow within the system (Equation 9). The heat exchanger had no heat source or sink, so, there were no additional terms and it did not have baffles. Flow was laminar, so turbulence was neglected. These equations are built into ANSYS Fluent and no customization was done and user-defined functions (UDFs) were not employed.

The continuity equation:

$$\frac{\partial u}{\partial x}+\frac{\partial v}{\partial y}+\frac{\partial w}{\partial z}=0 \tag{5}$$

Momentum equations:

In the x-axis; $u\frac{\partial u}{\partial x}+v\frac{\partial u}{\partial y}+w\frac{\partial u}{\partial z}=-\frac{1}{\rho}\frac{\partial p}{\partial x}+\boldsymbol{v}\left(\frac{\partial^2 u}{\partial x^2}+\frac{\partial^2 u}{\partial y^2}+\frac{\partial^2 u}{\partial z^2}\right)$ (6)

In the y-axis; $u\frac{\partial v}{\partial x}+v\frac{\partial v}{\partial y}+w\frac{\partial v}{\partial z}=-\frac{1}{\rho}\frac{\partial p}{\partial y}+\boldsymbol{v}\left(\frac{\partial^2 v}{\partial x^2}+\frac{\partial^2 v}{\partial y^2}+\frac{\partial^2 v}{\partial z^2}\right)$ (7)

In the z-axis; $u\frac{\partial w}{\partial x}+v\frac{\partial w}{\partial y}+w\frac{\partial w}{\partial z}=-\frac{1}{\rho}\frac{\partial p}{\partial z}+\boldsymbol{v}\left(\frac{\partial^2 w}{\partial x^2}+\frac{\partial^2 w}{\partial y^2}+\frac{\partial^2 w}{\partial z^2}\right)$ (8)

Energy equation:

In the y-axis; $u\frac{\partial T}{\partial x}+v\frac{\partial T}{\partial y}+w\frac{\partial T}{\partial z}=-\frac{1}{\rho}\frac{\partial p}{\partial y}+{}^{k}/_{\rho c_p}\left(\frac{\partial^2 T}{\partial x^2}+\frac{\partial^2 T}{\partial y^2}+\frac{\partial^2 T}{\partial z^2}\right)$ (9)

where u, v, w represents the components of velocity. The kinematic viscosity of the fluid was denoted as v, while p is pressure and ρ density.

2.4 Meshing

ANSYS meshing was used to divide the geometry into elements and nodes. The mesh consisted of tetrahedral elements and was properly refined for computational accuracy. There were 25,682 nodes with 16,262 elements. The proximity of edges and features of the geometry were also considered. Figure 3a shows the end of the DPHE mesh. It can be observed that there were no overlapping nodes and the elemental shapes were finely fitted within the geometry. The outlines of the inner pipe, cold and hot fluid can be traced. The side mesh of the geometry can be seen in Figure 3b. Elements and nodes were neatly arranged in a linear manner. These features are clearly defined in Figure 3c.

2.5 Boundary conditions

The DPHE was subjected to the following conditions before thermal analysis:

i. Outer walls: Adiabatic/insulated boundary. There was no heat flux or heat leakage into the environment, therefore it was assumed the heat exchanger was perfectly lagged.
ii. Hot inlet: A fixed inlet temperature of 415 K was used. This temperature did not vary. Also, a mass flow rate of 0.87 kg/s was specified.
iii. Hot outlet: The temperature of the hot fluid at the outlet of the inner pipe was to be determined. In ANSYS Fluent, a pressure-outlet boundary condition was specified.
iv. Cold inlet: The cold fluid entered the annulus at a temperature of 300 K at a mass flow rate of 0.90 kg/s.
v. Cold outlet: The cold fluid's outlet temperature was to be determined. A pressure outlet boundary condition was specified following a procedure similar to that for the hot fluid.
vi. Inner pipe walls: Heat transfer through the inner pipe wall was by conduction. Heat was absorbed from the hot fluid and rejected to the cold fluid. The temperature and heat flux were not specified. Heat flux at the wall was zero, so for both sides of the inner pipe, the no-slip boundary condition was specified.

2.6 Effectiveness

The performance parameter of the heat exchanger was estimated using Equation 10.

$$\varepsilon=\frac{actual\ heat\ transfer}{maximum\ possible\ heat\ transfer}=\frac{Q}{Q_{max}} \tag{10}$$

The actual energy balance can be expressed by Equation 11.

$$\dot{m}_{hot}C_p^{hot}(T_{inlet}^{hot}-T_{outlet}^{hot})=\dot{m}_{cold}C_p^{cold}(T_{outlet}^{cold}-T_{inlet}^{cold}) \tag{11}$$

The maximum possible temperature rise was estimated using Equation 12.

$$\Delta T_{max}=T_{inlet}^{hot}-T_{inlet}^{cold} \tag{12}$$

Hence the energy balance can be rewritten in Equation 13.

$$\dot{m}_{hot}C_p^{hot}\Delta T_{max}=\dot{m}_{cold}C_p^{cold}\Delta T_{min} \tag{13}$$

where ΔT_{min} is the difference between the temperatures at the hot inlet and cold outlet.

The heat loss through can be determined through the difference in the temperature at the ends of the pipes and the mass flow rates of the fluids. Thus, it can be computed using either Equation (14) or (15).

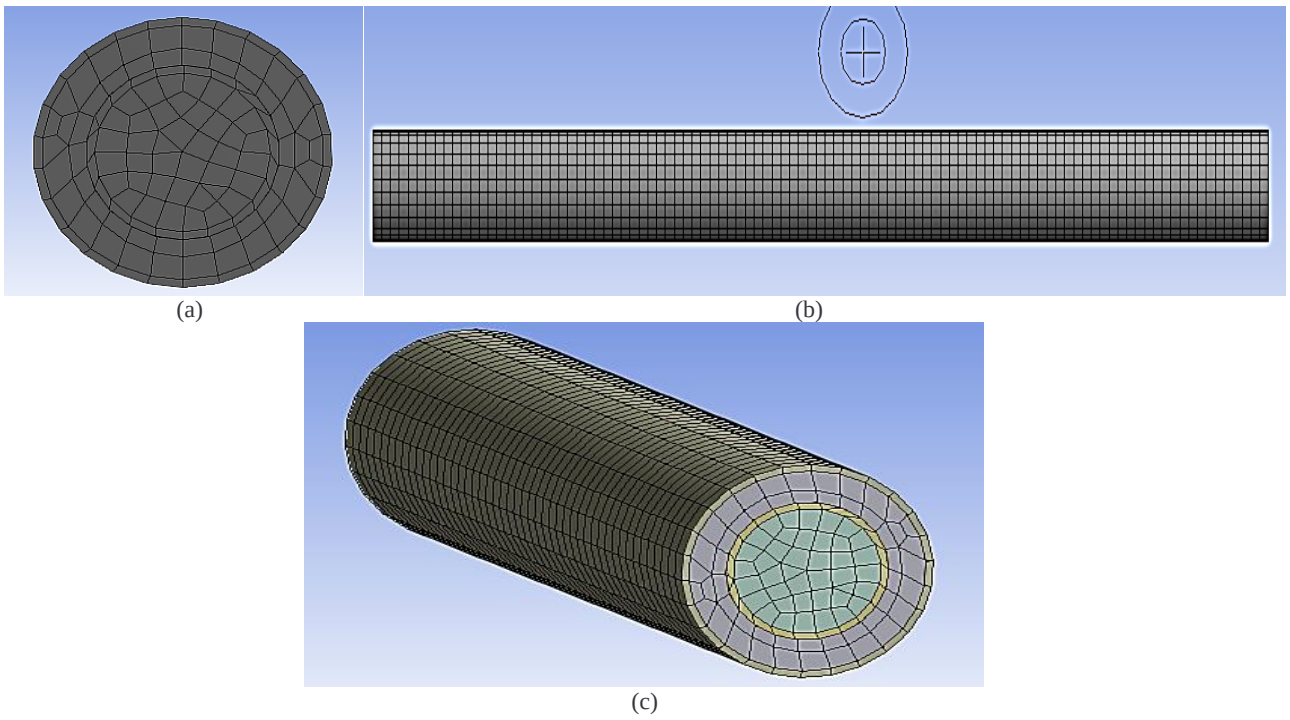

Figure 3 DPHE mesh, (a) cross-section, (b) side and (c) isometric views

Table 4 Validation results for outlet temperatures

Boundary	Prathyusha et al. [47]	This study	% Difference
Cold outlet	306.77 K	306.75 K	0.01%
Hot outlet	407.12 K	410.00 K	0.71%

$$Q = \dot{m}C_p^{hot}\left(T_{inlet}^{hot} - T_{outlet}^{hot}\right) \quad (14)$$

$$Q_{max} = \dot{m}C_p^{hot}\left(T_{inlet}^{hot} - T_{inlet}^{cold}\right) \quad (15)$$

3. Results and discussion

3.1 Model validation

The data and geometry used by Prathyusha et al. [47] were employed to test the simulation model for accuracy and reliability. The simulation results for the inlet and outlet temperatures corroborated the report of Prathyusha et al. [47] (Table 4) within 1%. The mass flow rates for the hot and cold fluids were 0.87 and 0.9 kg/s, respectively.

It can be clearly seen that the computational error was small for both the computed cold and hot fluid temperatures at their outlets. The percentage error of the model in this study was less than 1%, demonstrating high reliability and accuracy [48]. It can be used to simulate a DPHE and similar heat exchangers. The use of a water-copper oxide nanofluid as the cold fluid in the DPHE under study can now be performed.

3.2 Fluid properties

The thermal properties and density of the cold fluid were enhanced with the addition of nanoparticles. Nanoparticle volume fractions were varied from the control sample of $\emptyset = 0$ to $\emptyset = 0.1\%$ with a step size increment of 0.025%. The nanoparticles were usually added in small fractions to evenly disperse them within the bulk of the base fluid. The properties of the fluids containing nanoparticles in small fractions can then be evaluated as a single fluid. The effect of nanoparticle volume fraction on the viscosity is presented in Figure 4a.

The viscosity of the cold fluid increased almost linearly with the content of CuO nanoparticles, in line with the behaviour of Al_2O_3, TiO_2, and SiO_2 reported by Hussein et al. [24]. Without the CuO nanoparticles, (i.e., Ø=0), the fluid viscosity was 1×10^{-3} kg/ms. With the introduction of the nanoparticles, the fluid viscosity increased to 1.07×10^{-3}, 1.15×10^{-3}, 1.24×10^{-3} and 1.3×10^{-3} kg/ms for CuO volume fractions of 0.025%, 0.050%, 0.075%, and 0.1%, respectively. It can be argued that an increase in viscosity will provide greater flow resistance which will, in turn, require more pumping power. When the values of the viscosity increments were carefully selected, the change observed was very small – less than 3×10^{-4} kg/ms (Figure 4a). The nanoparticles had little effect when they were added in small quantities. According to Kumar et al. [49], the viscosity of a CuO nanofluid increased with the nanoparticle concentration at a constant temperature, but decreased as temperature was increased at the same concentration.

Figure 4b shows the effect of CuO volume fraction on the thermal conductivity of the cold fluid. The thermal conductivities of the nanofluids were 0.61, 0.65, 0.70, 0.75, and 0.80 W/mK for CuO volume fractions of 0.00%, 0.025%, 0.050%, 0.075%, and 0.1%, respectively. The thermal conductivity linearly increased by 30% with a 10% incremental increase in the volume fraction of CuO. This was comparable to a 27% increase in thermal conductivity with a 5% incremental increase of the volume fraction of Al_2O_3 reported by Baheta and Woldeyohannes [50]. The thermal conductivity of a material dictates the rate at which heat is transferred through a material. Usually, nanoparticles increase heat transfer surface area and provide for better heat flow [51]. This is possible because the nanoparticle material itself was metal-based. It is well established that metals have desirable thermal properties for heat transfer.

Figure 4c shows the effect on the SHC of adding CuO to cold fluid. Without the CuO nanoparticles, (i.e., Ø=0%), the SHC was 4.20 kJ/kg K. With the introduction of the nanoparticles, the SHC was reduced to 4.08, 3.99, 3.91, and 3.82 kJ/kg K for CuO volume fractions of 0.025%, 0.050%, 0.075% and 0.1%, respectively. It was observed that the SHC was reduced by 9.45% when the nanoparticle volume fraction was increased by 10%. Sekhar and Sharma [52] reported a similar trend for Al_2O_3. They found that the reduction in the SHC can be attributed to an

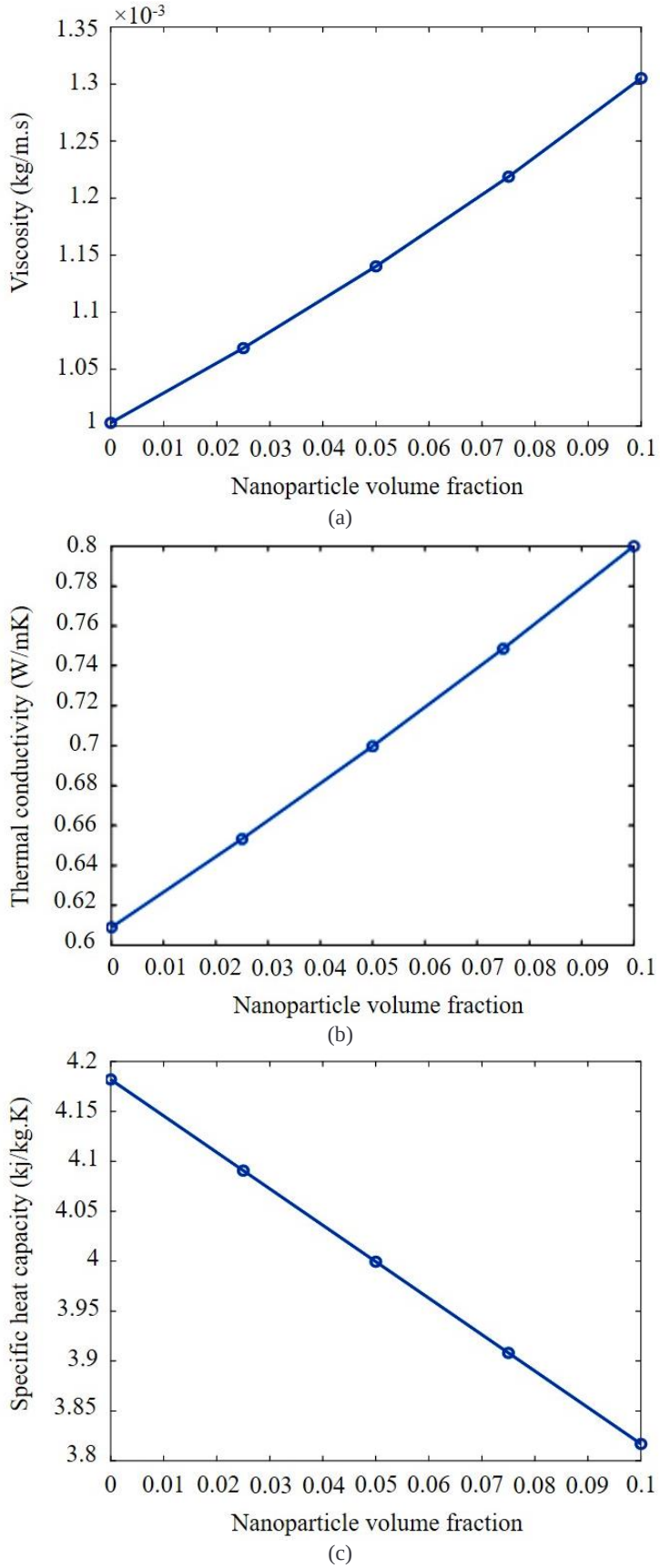

Figure 4 Effect of the CuO nanoparticles on the (a) viscosity, (b) thermal conductivity, (c) SHC of water at the cold fluid inlet

increase in thermal diffusivity. Although Zhou et al. [53] reported an increase in the SHC of a CuO nanofluid, the presence of ethylene glycol in their experiments may have been responsible for this increase. The value of the specific heat capacity of a substance provides information on its heat storage capability. Therefore, as the SHC of the cold fluid was reduced, heat was transferred more rapidly, thereby increasing the thermal efficiency of the DPHE. Factors such as surface area, the size of nanoparticles and agglomeration of nanoparticles within a nanofluid influenced the SHC.

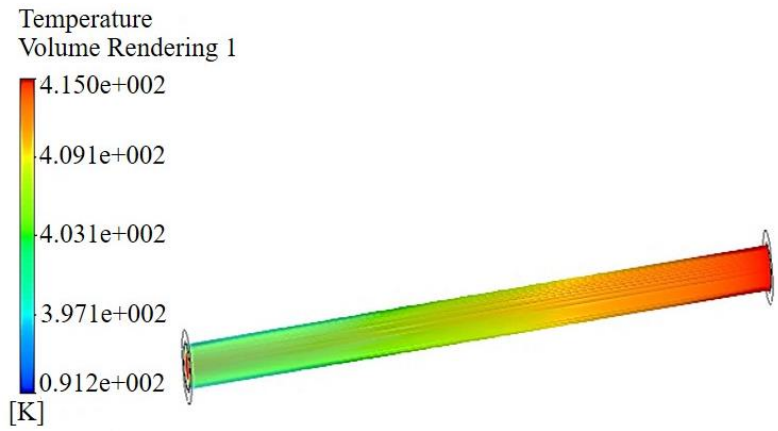

Figure 5 Temperature distribution in the hot fluid pipe for $\emptyset = 0\%$

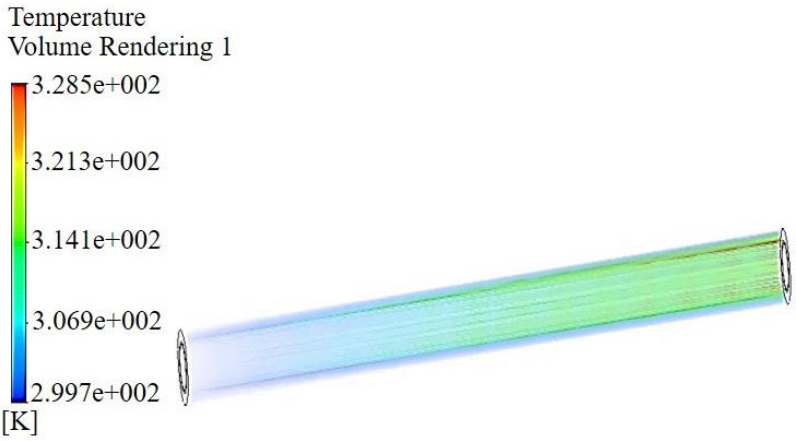

Figure 6 Temperature distribution in the cold fluid pipe for $\emptyset = 0\%$

3.3 Temperature distribution

The temperature distribution within the hot and cold fluids of the DPHE was also investigated. Before the CFD simulation was performed, the temperatures of the hot and cold outlets remained unknown. These temperatures are important parameters needed to evaluate the performance of the DPHE. They were used in estimating the effectiveness of the DPHE and the quantity of heat transferred from the hot to the cold fluid. Figures 5 and 6 present the temperature distribution within the hot and cold fluids, respectively, during a counter-current flow.

In the hot pipe, there was a 21.5 K reduction in temperature as the fluid flowed from the hot inlet to the hot outlet (Figure 5), while in the cold pipe, there was 28.5 K increase in temperature as the fluid flowed from the cold inlet to the cold outlet (Figure 6). At the preselected flow, a pure laminar flow was observed as the relative fluid velocity remained low [54]. In this arrangement, bulk fluid mixing was low as was the coefficient of convective heat transfer, confirming the report of Albadr et al. [55]. Low velocity, however, ensured an increased thermal performance as the fluid flowed through the DPHE [54, 56]. Simulations for all cases of $\emptyset = 0\%$ to $\emptyset = 0.1\%$ were done and the unknown outlet temperatures were determined. Figures 7a and b show the maximum temperatures of the pipe at the hot and cold fluid outlets, respectively.

From Figure 7a, the temperature at the hot fluid outlet was reduced with an increased volume fraction of CuO as a result of changes in the properties of the cold fluid. The maximum temperatures of the nanofluid were 391.3, 390.8, 390.2, 389.6, and 389.1 K for CuO volume fractions of 0.00%, 0.025%, 0.050%, 0.075%, and 0.1%, respectively. Conversely, the maximum temperature at the cold fluid outlet increased with the volume fraction of CuO. With no CuO nanoparticles, the maximum temperature at the cold fluid outlet was 328.5 K, while with the CuO nanoparticles, the maximum cold outlet temperature increased to 329.0, 329.6, 329.8 and 330.3 K for CuO volume fractions of 0.025%, 0.05%, 0.075% and 0.1%, respectively (Figure 7b). The convective heat transfer within the cold fluid increased because the CuO volume fraction increased the surface area available for heat transfer. This, in turn, enhanced the rate of thermal conduction through the solid walls of the inner pipe. The inner pipe then absorbed heat faster, thereby fostering heat loss from the hot fluid.

The presence of CuO in the cold fluid reduced its SHC [52] and therefore enhanced heat transfer. In turn, the cold fluid absorbed more heat, increasing it temperature rise, and therefore, the heat transferred across the inner pipe wall of the DPHE. The temperature of the outer pipe and the cold fluid gradually increased along the length of the DPHE from the inlet to the outlet point. At the outlet, the maximum temperature was attained.

3.4 DPHE performance

The performance of the DPHE was estimated using the inlet and outlet temperatures. The effectiveness of the heat exchanger was computed for all cases and plotted against the nanoparticle volume fraction (Figure 8). Effectiveness increased linearly from a value of 0.212 to above 0.254 as the volume fraction of CuO was raised from 0 to 0.1. This increase in effectiveness means that heat transfer across the heat exchanger approached the maximum overall heat transfer coefficient [1]. A DPHE can be optimized based on this parameter by evaluating the effect of the CuO volume fraction.

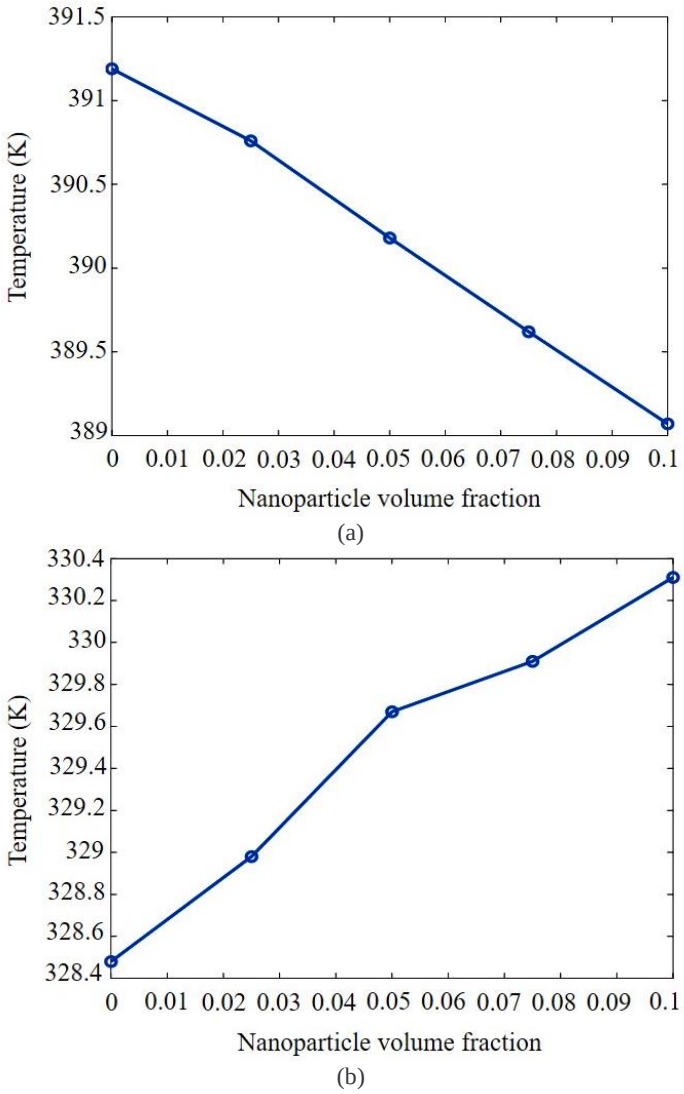

Figure 7 Maximum temperature with varying nanoparticle volume fractions at the (a) hot and (b) cold fluid outlets

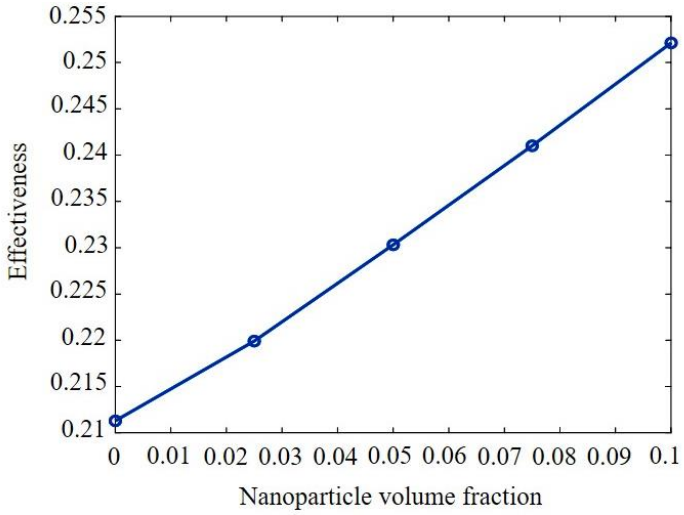

Figure 8 Effect of CuO nanoparticles on the effectiveness of a DPHE

The heat transferred across the DPHE is plotted against the volume fraction of CuO in Figure 9. It was 5.08, 5.17, 5.30, 5.41 and 5.54 kW for CuO volume fractions of 0.00%, 0.025%, 0.050%, 0.075% and 0.1%, respectively. The rate of heat transfer across the DPHE increased linearly with incremental increases in the volume fraction of CuO. This followed the same trend as the temperature and effectiveness of the DPHE. With these results, this study, therefore, reiterates that nanoparticles are effective in improving heat transfer and heat exchanger performance. Srinivas and Vinod [57] reported an enhanced rate of heat transfer with the use of a CuO nanofluid in a shell and helical coil heat exchanger. Similarly, Wongcharee and Eiamsa-ard [58]

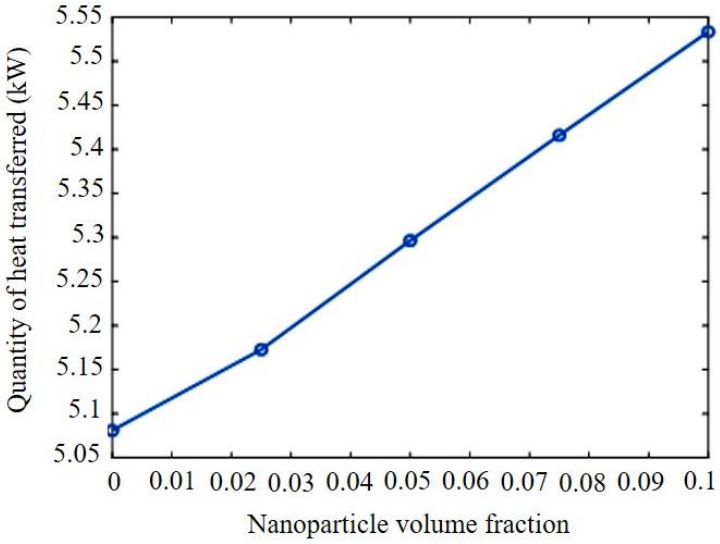

Figure 9 Effect of CuO volume faction on heat transfer

observed this for a CuO/water nanofluid in a corrugated tube equipped with twisted tapes, as did Radkar et al. [59] for a ZnO nanofluid in a helical copper tube heat exchanger. These studies revealed that this concept can be applied to heat exchangers of more complex geometries.

4. Conclusions

This study investigated the effects of cold fluid and a mixture of cold fluid with various volume fractions of CuO nanoparticles on heat transfer in a DPHE. To achieve this, the heat exchanger was modelled with ANSYS 16.0 and subjected to computational fluid dynamics analysis. With an increase in the volume fraction of CuO nanoparticles from 0% to 0.1% in the nanofluid, the average viscosity was 3×10^{-4} kg/ms and the thermal conductivity increased by 30% (0.61 to 0.80 W/mK). Concurrently, the SHC was reduced by 9.45% (from 4.20 to 3.82 kJ/kg K), the DPHE effectiveness increased gradually from 0.212 to 0.254, while the heat transfer increased from 5.08 to 5.54 kW. Therefore, introducing CuO nanoparticles enhanced heat transfer, corroborating previous studies.

5. References

[1] Lunsford KM. Increasing heat exchanger performance. Texas: Bryan Research and Engineering Inc; 1998.
[2] Picon-Nunez M, Melo-Gonzalez JC, Garcia-Castillo JL. Use of heat transfer enhancement techniques in design of heat exchangers. In: Gómez LC, Velázquez Flores VM, editors. Advances in heat exchanges. London: IntechOpen; 2018. p. 1-18.
[3] Siddique M, Khaled A-RA, Abdulhafiz NI, Boukhary AY. Recent advances in heat transfer enhancements: a review report. Int J Chem Eng. 2010;2010:106461.
[4] Sharma S, Kaushal R, Siddhu V. A review of heat transfer augmentation in a heat exchanger using active and passive method. IJIRT. 2018;5(2):70-4.
[5] Alam I, Rohit S. Heat transfer augmentation in a double pipe heat exchanger using water-beryllium oxide based nanofluid using CFD. IJIRT. 2018;5(1):324-9.
[6] Natarajan A, Venkatesh R, Gobinath S, Devakumar L, Gopalakrishnan K. CFD simulation of heat transfer enhancement in circular tube with twisted tape insert by using nanofluids. Mater Today Proc. 2020;21:572-7.
[7] Khan M, Hashim, Hafeez A. A review on slip-flow and heat transfer performance of nanofluids from a permeable shrinking surface with thermal radiation: dual solutions. Chem Eng Sci. 2017;173:1-11.
[8] Hafeez A, Khan M, Ahmed J. Stagnation point flow of radiative Oldroyd-B nanofluid over a rotating disk. Comput Meth Programs Biomed. 2020;191:105342.
[9] Hashim, Hafeez A, Alshomrani AS, Khan M. Multiple physical aspects during the flow and heat transfer analysis of Carreau fluid with nanoparticles. Sci Rep. 2018;8:17402.
[10] Aghayari R, Maddah H, Zarei M, Dehghani M, Mahalle SGK. Heat transfer of nanofluid in a double pipe heat exchanger. Int Sch Res Notices, 2014;2014:1-7.
[11] Hamid A, Hashim, Khan M, Hafeez A. Unsteady stagnation-point flow of Williamson fluid generated by stretching/shrinking sheet with Ohmic heating. Int J Heat Mass Tran. 2018;126:933-40.
[12] Hashim, Hafeez A, Alshomrani AS, Khan M. Heat transport features of magnetic water–graphene oxide nanofluid flow with thermal radiation: stability Test. Eur J Mech B Fluid. 2019;76:434-41.
[13] Hafeez A, Khan M, Ahmed J. Thermal aspects of chemically reactive Oldroyd-B fluid flow over a rotating disk with Cattaneo–Christov heat flux theory. J Therm Anal Calorim. 2020;140:1-11.
[14] Hafeez A, Khan M, Ahmed J. Flow of Oldroyd-B fluid over a rotating disk with Cattaneo-Christov theory for heat and mass fluxes. Comput Meth Programs Biomed. 2020;191:105374.
[15] Khan M, Hafeez A, Ahmed J. Impacts of non-linear radiation and activation energy on the axisymmetric rotating flow of Oldroyd-B fluid. Phys Stat Mech Appl. 2020:124085.
[16] Huminic G, Huminic A. Application of nanofluids in heat exchangers: a review. Renew Sustain Energ Rev. 2012;16(8):5625-38.
[17] Fsadni AM, Whitty JPM, Adeniyi AA, Simo J, Brooks HL. Review on the application of nanofluids in coiled tube heat exchangers. In: Ahmed W, Jackson MJ, editors. Micro and Nanomanufacturing. Cham: Springer; 2017. p. 443-65.
[18] Ramis MK, Pasha J, Shebeer R. Heat transfer enhancement using CuO nanofluids – the effect of sonication time on the paradoxical behaviour. Int J Eng Sci Tech. 2012;4(7):3514-20.
[19] Narendra G, Kumara Swami Gupta AVSS, Krishnaiah A, Satyanarayana MGV. Experimental investigation on the preparation and application of nanofluids. Mater Today Proc. 2017;4(2):3926-31.

[20] Asadi A, Poufattah F, Miklos S, Afrand M, Zyla G, Ahn HS, et al. Effect of sonication characteristics on stability, thermophysical properties, and heat transfer of nanofluids: a comprehensive review. Ultrason Sonochem. 2019; 58:104701.
[21] Tiwari AK, Ghosh P, Sarkar J, Dahiya H, Parekh J. Numerical investigation of heat transfer and fluid flow in plate heat exchanger using nanofluids. Int J Therm Sci. 2014;85:93-103.
[22] Sundar LS, Sharma KV, Singh MK, Sousa ACM. Hybrid nanofluids preparation, thermal properties, heat transfer and friction factor–a review. Renew Sustain Energ Rev. 2017;68:185-98.
[23] Demir H, Dalkilic AS, Kürekci NA, Duangthongsuk W, Wongwises S. Numerical investigation on the single phase forced convection heat transfer characteristics of TiO_2 nanofluids in a double-tube counter flow heat exchanger. Int Comm Heat Mass Tran. 2011;38(2):218-28.
[24] Hussein AM, Sharma KV, Bakar RA, Kadirgama K. The effect of nanofluid volume concentration on heat transfer and friction factor inside a horizontal tube. J Nanomater. 2013;2013:859563.
[25] Ghalib L, Rahma NM, Eweed KM, Al-Kamal AK. Flow and Heat transfer experimental investigation of nanofluid in a double pipe heat exchanger. IOP Conf Ser: Mater Sci Eng. 2018;454:012150.
[26] Huminic, G, Huminic, A. Heat transfer characteristics in double tube helical heat exchangers using nanofluids. Int J Heat Mass Tran. 2011;54(19-20):4280-7.
[27] Shirvan Milani K, Mamourian M, Mirzakhanlari S, Ellahi R. Numerical investigation of heat exchanger effectiveness in a double pipe heat exchanger filled with nanofluid: a sensitivity analysis by response surface methodology. Powder Tech. 2017;313:99-111.
[28] Mozafarie SS, Javaherdeh K, Ghanbari O. Numerical simulation of nanofluid turbulent flow in a double-pipe heat exchanger equipped with circular fins. J Therm Anal Calorim. 2021;143:4299-311.
[29] Bahmani MH, Sheikhzadeh G, Zarringhalam M, Akbari OA, Alrashed AAAA, Shabani Gas, et al. Investigation of turbulent heat transfer and nanofluid flow in a double pipe heat exchanger. Adv Powder Tech. 2018;29(2):273-82.
[30] Ravi Kumar NT, Bhramara P, Addis BM, Sundar LS, Singh MK, Sousa ACM. Heat transfer, friction factor and effectiveness analysis of Fe3O4/water nanofluid flow in a double pipe heat exchanger with return bend. Int Comm Heat Mass Tran. 2017;81:155-63.
[31] Barewar SD, Chougule SS. Thermal performance of double-pipe concentric heat exchanger with synthesized zinc oxide nanofluid. In: Singh S, Ramadesigan V, editors. Advances in Energy Research, Vol 1. Singapore: Springer; 2020. p. 705-13.
[32] Pattanayak B, Mund A, Jayakumar JS, Parashar K, Parashar SKS. Estimation of Nusselt number and effectiveness of double-pipe heat exchanger with Al2O3–, CuO–, TiO2–, and ZnO–water based nanofluids. Heat Tran. 2020;49(4):2228-47.
[33] Arya H, Sarafraz MM, Pourmehran O, Arjomandi M. Performance index improvement of a double-pipe cooler with MgO/water-ethylene glycol (50:50) nano-suspension. Propuls Power Res. 2020;9(1):75-86.
[34] Dalkılıç AS, Mercan H, Özçelik G, Wongwises S. Optimization of the finned double-pipe heat exchanger using nanofluids as working fluids. J Therm Anal Calorim. 2021;143:859-78.
[35] Moradi A, Toghraie D, Isfahani AHM, Hosseinian A. An experimental study on MWCNT–water nanofluids flow and heat transfer in double-pipe heat exchanger using porous media. J Therm Anal Calorim, 2019;137(5):1797-807.
[36] Mukesh Kumar PC, Chandrasekar M. Heat transfer and friction factor analysis of MWCNT nanofluids in double helically coiled tube heat exchanger. J Therm Anal Calorim. In press 2020.
[37] Hashemi Karouei SH, Ajarostaghi SSM, Gorji-Bandpy M, Hosseini Fard SR. Laminar heat transfer and fluid flow of two various hybrid nanofluids in a helical double-pipe heat exchanger equipped with an innovative curved conical turbulator. J Therm Anal Calorim. 2021;143:1455-66.
[38] Omidi M, Farhadi M, Jafari M. A comprehensive review on double pipe heat exchangers. Appl Therm Eng. 2017; 110:1075-90.
[39] Dehankar PB, Pandhare KK, Vagare MJ, Nerlekar VM. A double pipe heat exchanger – fabrication and standardization. IJRITCC. 2015;3(4):1845-7.
[40] Al Shdaifat MY, Zulkifli R, Sopian K, Salih AA. Thermal and hydraulic performance of CuO/water nanofluids: a review. Micromachines. 2020;11(4):416.
[41] Marcelino EW, Riehl RR, Debora S de O. A review on thermal performance of CuO-water nanofluids applied to heat pipes and their characteristics. 15th IEEE Intersociety Conference on Thermal and Thermomechanical Phenomena in Electronic Systems (ITherm); 2016 May 31 - Jun 3; Las Vegas, USA. USA: IEEE; 2016. p. 1-11.
[42] Sahooli M, Sabbaghi S, Shariaty Niassar M. Preparation of CuO/water nanofluids using Polyvinylpyrolidone and a survey on its stability and thermal conductivity. Int J Nanosci Nanotechnol. 2012;8(1):27-34.
[43] Brinkman HC. The viscosity of concentrated suspensions and solutions. J Chem Phys. 1952;20(4):571.
[44] Mintsa HA, Roy G, Nguyen CT, Doucet D. New temperature dependent thermal conductivity data for water based nanofluids. Therm Sci. 2009;48:363-71.
[45] Zhou S-Q, Ni R. Measurement of the specific heat capacity of water-based Al_2O_3 nanofluid. Appl Phys Lett. 2008;92:093123.
[46] Pak BC, Cho Y. Hydrodynamic and heat transfer study of dispersed fluids with submicron metallic oxide particle. Exp Heat Tran. 1998;11(2):151-70.
[47] Prathyusha BGR, Janjanam N, Narasimha KVR, Sandeep G. Numerical investigation on shell & tube heat exchanger with segmental and helix baffles. IJMPERD. 2018;8:183-92.
[48] Navarro HA, Cabezas-Gomez LC. Effectiveness-NTU computation with a mathematical model for cross-flow heat exchangers. Braz J Chem Eng. 2007;24(4):509-21.
[49] Kumar S, Sokhal GS, Singh J. Effect of Cuo-distilled water based nanofluids on heat transfer characteristics and pressure drop characteristics. Int J Eng Res Appl. 2014; 4(9):28-37.
[50] Baheta AT, Woldeyohannes AD. Effect of particle size on effective thermal conductivity of nanofluids. Asian J Sci Res. 2013;6(2):339-45.
[51] Das SK, Choi SUS, Patel HE. Heat transfer in nanofluids – a review. Heat Tran Eng. 2006;27(10):3-19.
[52] Sekhar YR, Sharma KV. Study of the viscosity and specific heat capacity characteristics of water-based Al_2O_3 nanofluids at low particle concentration. J Exp Nanosci. 2015;10(2):86-102.
[53] Zhou LP, Wang BX, Peng XF, Du XZ, Yang YP. On the specific heat capacity of CuO nanofluid. Adv Mech Eng. 2010;2:172085.
[54] Ekramian E, Etemad SGh, Haghshenasfard M. Numerical investigations of heat transfer performance of nanofluids in flat plate solar collector. Int J Theor Appl Nanotech. 2014;2:30-9.
[55] Albadr J, Tayal S, Alasadi M. Heat transfer through heat exchanger using Al_2O_3 nanofluid at different concentrations. Case Stud Therm Eng. 2013;1(1): 38-44.

[56] Sarafraz MM, Safaei MR, Tian Z, Goodarzi M, Filho EPB, Arjomandi M. Thermal assessment of nano-particulate grapheme-water/ethylene glycol (WEF 60:40) nano-suspension in compact heat exchanger. Energies. 2012; 12(10):1929.

[57] Srinivas T, Vinod AV. Heat transfer enhancement using CuO / water nanofluid in a shell and helical coil heat exchanger. Procedia Eng. 2015;127: 1271-7.

[58] Wongcharee K, Eiamsa-ard S. Heat transfer enhancement by using CuO/water nanofluid in corrugated tube equipped with twisted tape. Int Commun Heat Mass Tran. 2012; 39(2):251-7.

[59] Radkar RN, Bhanvase BA, Barai DP. Sonawane SH. Intensified convective heat transfer using ZnO nanofluids in heat exchanger with helical coiled geometry at constant wall temperature. Mater Sci Energ Tech. 2019; 2(2): 161-70.